Mol Psychiatry. Author manuscript; available in PMC 2017 April 25.

Published in final edited form as:
Mol Psychiatry. 2017 May ; 22(5): 689–702. doi:10.1038/mp.2016.30.

Pharmacological enhancement of mGlu5 receptors rescues behavioral deficits in SHANK3 knock-out mice

Cinzia Vicidomini[1], **Luisa Ponzoni**[2], **Dmitry Lim**[3], **Michael Schmeisser**[4], **Dominik Reim**[2], **Noemi Morello**[5], **Daniel Orelanna**[1], **Alessandro Tozzi**[6], **Valentina Durante**[9], **Paolo Scalmani**[7], **Massimo Mantegazza**[8], **Armando A. Genazzani**[3], **Maurizio Giustetto**[5], **Mariaelvina Sala**[1,4], **Paolo Calabresi**[9], **Tobias M. Boeckers**[2], **Carlo Sala**[1], and **Chiara Verpelli**[1]

[1]CNR Neuroscience Institute, Milan, Milano

[2]BIOMETRA University of Milan, Milano

[3]Department of Pharmaceutical Sciences, Università degli Studi del Piemonte Orientale “Amedeo Avogadro”, Novara

[4]Institute for Anatomy and Cell Biology, Ulm University, Ulm

[5]Department of Neuroscience, University of Turin, Torino

[6]University of Perugia, Department of Experimental Medicine, Perugia

[7]U.O. of Neurophysiopathology and Diagnostic Epileptology, Foundation Istituto di Ricerca e Cura a Carattere Scientifico (IRCCS) Neurological Institute Carlo Besta, Milan

[8]Institute of Molecular and Cellular Pharmacology (IPMC), Laboratory of Excellence Ion Channel Science and Therapeutics (LabEx ICST), CNRS UMR7275 and University of Nice-Sophia Antipolis, Valbonne

[9]Department of Medicine, University of Perugia and Clinica Neurologica, Santa Maria della Misericordia Hospital, Perugia, Italy

Abstract

SHANK3 (also called PROSAP2) genetic haploinsufficiency is thought to be the major cause of neuropsychiatric symptoms in Phelan-McDermid syndrome (PMS). PMS is a rare genetic disorder that causes a severe form of intellectual disability (ID), expressive language delays and other autistic features. Furthermore, a significant number of *SHANK3* mutations have been identified in patients with Autism Spectrum disorders ASD, and *SHANK3* truncating mutations are associated with moderate to profound ID. The Shank3 protein is a scaffold protein that is located in the postsynaptic density (PSD) of excitatory synapses and is crucial for synapse development and plasticity. In this study, we investigated the molecular mechanisms associated with the ASD-like

Corresponding author: Chiara Verpelli PhD, CNR Neuroscience Institute, Via Vanvitelli 32, 20129 Milano, Tel. +39-0250317122, Fax +39-0250317132, c.verpelli@in.cnr.it.

Conflict of Interest
The authors declare they have no conflicts of interest.

Europe PMC Funders Author Manuscripts

behaviors observed in *Shank3Δ11*$^{-/-}$ mice in which exon 11 has been deleted. Our results indicate that Shank3 is essential to mediating mGlu5 receptor signaling by recruiting Homer1b/c to the PSD, specifically in the striatum and cortex. Moreover, augmenting mGlu5 receptor activity by administering 3-Cyano-*N*-(1,3-diphenyl-1*H*-pyrazol-5-yl)benzamide (CDPPB) ameliorated the functional and behavioral defects that were observed in *Shank3Δ11*$^{-/-}$ mice, suggesting that pharmaceutical treatments that increase mGlu5 activity may represent a new approach for treating patients that are affected by PMS and *SHANK3* mutations.

Introduction

SHANK3/PROSAP2 is considered to be the main gene that is associated with the neuropsychiatric symptoms experienced by patients with Phelan McDermid syndrome (PMS). PMS is characterized by a significant delay in expressive language, intellectual disability (ID), hypotonia, minor craniofacial dysmorphisms, increased tolerance to pain, epilepsy and autism-like features 1. Furthermore *SHANK3* truncating mutations have been identified in patients with autism spectrum disorders (ASD) 2. ASD is a complex neurodevelopmental disorder that is defined by repetitive, restricted behavioral patterns and impaired sociability and communication. These neuropsychiatric conditions are probably due to the altered formation and plasticity of synaptic connections, which can lead to dysfunctional neuronal communication. Therefore, understanding the functions of Shank3 in the brain is crucial to developing new pharmacological targets with which to treat patients with Shank3 mutations or deletions. Indeed, several *Shank3* KO mice were generated in which different regions of the gene were deleted 3–8. For a review, please see 9.

Shank proteins (encoded by three genes, Shank 1−3) are scaffold proteins that are located in the postsynaptic density (PSD) of glutamatergic synapses. They are essential for dendritic spine development and plasticity. Overexpression of Shank1 in hippocampal neurons accelerated the maturation of filopodial−like protrusions in mature spines and promoted the enlargement of mature spines 10, 11. However, smaller dendritic spines, weaker synaptic transmission, and altered spatial learning have been observed in mice lacking Shank1 12. Shank3 overexpression in cerebellar granule cells induced dendritic spine and synapse formation by recruiting different subtypes of glutamate receptors, whereas inhibiting Shank3 expression in hippocampal neurons reduced the number of dendritic spines 13, 14.

Shanks proteins, which are composed of five protein-protein interaction domains, including N-terminal ankyrin repeats (ANK), a Src Homology 3 domain (SH3), a PDZ domain, a proline-rich region (Pro-rich), and a sterile alpha motif domain (SAM) at the C-terminus, interact with more than 30 synaptic proteins, including cytoskeletal proteins, cell adhesion proteins, and ionotropic and metabotropic glutamate receptors. A major complex is formed by interactions between the Pro-rich region of Shank with the EVH1 (Ena-VASP homology 1) domain of Homer proteins. Through this interaction and through the multimerization of Homer1b/c via its C-terminal coiled-coil domains, Shank stabilizes mGlu1 and mGlu5 at excitatory synapses and regulates its inositol-1,4,5-trisphosphate receptor (IP3R)-mediated downstream pathway 15–18.

Europe PMC Funders Author Manuscripts

Interestingly, the direct alteration of Homer1 and mGlu5 gene expression and function has been identified as a risk factor for ASD 19 , and different studies have linked Homer proteins to mGlu5 receptor-mediated synaptic plasticity and ASD 20, 21. mGlu5 proteins are highly expressed postsynaptically in the cortex, striatum and hippocampus 22–24.

Our previous studies demonstrated that in rat hippocampal cell cultures, mGlu5 receptor expression and function were strongly affected when Shank3 expression was downregulated using a specific shRNA 14. However, it is not clear whether in vivo Shank3 deletion caused these impairments in mGlu5 functions.

In this study, we investigated the molecular mechanisms that are associated with the ASD-like behaviors observed in *Shank3Δ11*$^{-/-}$ mice, which were generated by deleting exon 11 and which are characterized by the absence of the three major and higher MW isoforms of Shank3 25.

Our data indicate that, specifically in striatum and cortex, Shank3 performs an essential function in mediating mGlu5 receptor signaling by recruiting Homer1b/c to the PSD. Moreover, our results suggest that augmenting mGlu5 receptor activity using CDPPB ameliorated the functional and behavioral defects observed in *Shank3Δ11*$^{-/-}$ mice.

Materials and Methods

Mice

The *Shank3Δ11*$^{-/-}$ mice were generated as previously described by Schemeisser et al. 25 and re-derived in a C57BL/6 background (Charles River Laboratories, Calco, Italy). They were housed under constant temperature (22 ± 1°C) and humidity (50%) conditions with a 12 h light/dark cycle and provided with food and water ad libitum. Using heterozygous mice for breeding, we derived wild type and knockout littermates.

Cell culture preparation and transfection of primary rat and mouse cortical neurons

Rat cortical neuronal cultures were obtained from 18- to 19-day-old rat embryos as previously described, with minor modifications 11, 14. Neurons were grown in B27 medium that was prepared in the laboratory in 12- or 6-well petri dishes (Primo).

Mouse cortical neurons were prepared from E18 embryos, grown in 12- or 6-well petri dishes (Primo) and maintained in Neurobasal B27-supplemented medium (Life Technologies). Rat cortical neurons were transfected using Lipofectamine 2000 on day 11 (DIV11), and the experiments were performed on DIV13-15.

Immunocytochemistry and image analysis

Mouse cortical neurons were fixed at DIV13 in 100% methanol at -20°C for 10 minutes. Rat cortical neurons were transfected at DIV 11 and fixed at DIV15 in 4% paraformaldehyde. Primary antibodies (anti-Homer1, provided by Enjoom Kim Laboratory, KAIST Institute, Sout Korea and anti-Bassoon, Enzo Life Sciences, cat. ADI-VAM-PS003-F) and secondary antibodies were applied in GDB Buffer in PBS (30 mM phosphate buffer, pH 7.4, 0.2% gelatin, 0.5% Triton X-100, and 0.8 M NaCl; all from Sigma-Aldrich).

Confocal images were obtained using a confocal microscope (Zeiss 510 Confocal Microscope, a gift from Fondazione Monzino) with a 63× objective and sequential-acquisition setting at a resolution of 1024 × 1024 pixels. A total of 16 neurons (cortical neurons fixed at DIV 15) for each genotype (WT and KO) were randomly chosen for quantification from 4 to 10 coverslips from three independent experiments. Morphometric measurements were performed using MetaMorph image analysis software. Colocalization was measured by using color-separating Homer and Bassoon channels, manually setting a threshold level for each channel (identical for each neuron), and then determining the overlapping area using MetaMorph analysis.

Morphometric and colocalization analyses were performed by investigators who were blind to the experimental conditions. Measurements are expressed as the means ± SEM.

For the immunodetection of postsynaptic density markers on brain sections, the mice were anesthetized intraperitoneally using Avertin (Sigma-Aldrich) and then decapitated. The brains were rapidly excised and manually cut into coronal slabs that were fixed via immersion in ice-cold paraformaldehyde (4% in 0.1 M phosphate buffer, PB, pH 7.4) for 30 min 26. After fixation, the tissue slabs were rinsed in PB, cryoprotected via immersion in ascending sucrose solutions (10%, 20% and 30%), cut into 20-μm sections with a cryostat, mounted on gelatin-coated slides and stored for a maximum of one month at −20°C until immunolabeling was performed. Following blocking in normal donkey serum (NDS, 3% in PBS with 0.5% Triton X-100), the sections were incubated with primary antibodies diluted in PBS containing 3% NGS and 0.5% Triton X-100 overnight at 4°C (anti-PSD-95 NeuroMab, Ca, USA cat. 75-028 and anti-Homer1 provided by Enjoom Kim Laboratory, KAIST Institute, Sout Korea). The sections were then washed and incubated with secondary antibodies (cyanine-derived Cy3 anti-mouse, Alexa Fluor 488 anti-rabbit, both 1:1000; Jackson ImmunoResearch, West Grove, PA) that were diluted in 3% NGS and 0.5% Triton X-100 in PBS for 1 hour at room temperature. The sections were rinsed again and coverslipped with Dako fluorescence mounting medium (Dako Italia, Italy). For quantitative analysis of Homer1-immunoreactive puncta and colocalization studies, 5 serial optical sections (using a 0.5-μm Z-step size) were acquired from sections including layers 2-3 of the primary somatosensory cortex (S1), the CA1 region of the hippocampus (stratum radiatum) and the dorsal striatum (caudate and putamen nuclei) using a laser scanning confocal microscope (LSM5 Pascal; Zeiss) with a 100× objective (1.4 numerical aperture) and the pinhole set at 1 Airy unit. The density of the immunolabeled puncta was determined by manually counting postsynaptic clusters in neuropilar areas using dedicated software (Imaris, Bitplane, Zurich, CH) and expressed as puncta/100 μm^2.

Subcellular Fractionation and Western Blot analysis

Subcellular fractionation of brain tissues was performed according to *Distler et al., Proteomics, 2014*, with some modifications. All steps were performed at 4°C. In brief, tissues were homogenized in buffer A containing 0.32 M sucrose and 5 mM HEPES (pH7.4) and centrifuged at 1.000 x g. The supernatant (S1) was further centrifuged at 12.000 x g, and a pellet containing the crude membrane fraction (P2) was obtained. This fraction was solubilized in buffer B containing 0.32 M sucrose and 5 mM Tris (pH 8.1) and loaded onto a

discontinuous sucrose step gradient (0.85 M/1.0 M/1.2 M). After centrifugation at 85.000 x g, the synaptosomes (Syn) were collected from the 1.0 M/1.2 M interface and incubated with buffer C containing 0.32 M sucrose, 12 mM Tris (pH 8.1) and 1% Triton X-100. After centrifugation at 32.800 x g, the PSD pellet was collected and solubilized in H2O.

Equal amounts (10 μg) of each sample were separated using SDS-PAGE and subsequently blotted on nitrocellulose membranes according to standard protocols. Incubation with a primary antibody (β-actin Sigma, cat. A5316; Homer1b/c, SynapticSystems, cat. 160022,; mGluR5, Millipore, cat. AB5675; Shank3, Santa Cruz Biothecnology, cat. H-160; β3-tubulin, Covance, cat. PRB-435P) was followed by treatment of the membrane with HRP-conjugated secondary antibodies (swine anti-rabbit, 1:1000 or rabbit anti-mouse, 1:3000; both Dako, Hamburg, Germany), and the signal was visualized using Pierce ECL Western Blotting Substrate and further detected using a MicroChemi 4.2 machine. All signals were quantified using Gel analyzer software (www.gelanalyzer.com/) and normalized against the values of the respective signal for β-actin.

Immunoprecipitation Assay

PSD-enriched preparations (as previously described) of different brain regions (cortex, hippocampus and striatum) from P60 WT and KO mice were incubated at 4°C overnight with protein A-Sepharose beads (GE Healthcare) conjugated to 10 μg/ml of Homer1b/c (Santa Cruz cat. H-342) or of PSD-95 (NeuroMab, Ca, USA cat. 75-028) or control IgG (10 μg/ml) antibodies. The beads were then washed three times with RIPA buffer, re-suspended in sample buffer, warmed at 65°C for 10 minutes and analyzed using SDS-PAGE. Western blot analysis was performed using mGlu5 (Millipore, cat. AB5675), SynGAP (Cell Signaling cat. D78B11) andGluN2A (Sigma cat. G9038) primary antibodies.

FURA-2 Single Cell Ca^{2+} Imaging

For Ca^{2+} measurements, 0.3 mln neurons were plated onto 24-mm round coverslips in 6-well plates. At DIV12-DIV14, the plates were loaded with 5 μM Fura-2 AM (Life Technologies, Milan, Italy) containing 0.002% Pluronic F-127 (Life Technologies) and 10 μM sulfinpyrazone (Sigma) in Krebs-Ringer modified buffer (KRB solution: 125 mM NaCl, 5 mM KCl, 1 mM Na_3PO_4, 1 mM $MgSO_4$, 2 mM $CaCl_2$ 5.5 mM glucose, and 20 mM HEPES, pH 7.4) for 30 min at room temperature (RT). The neurons were then washed twice in KRB, and the Fura-2 was allowed to de-esterify for another 30 min at RT. The coverslips were then mounted in the acquisition chamber of a Leica DMI6000 epifluorescent microscope equipped with an S Fluor 40x/1.3 objective. First, neurons expressing a GFP-tagged shShank3 or control (shCtrl) plasmid were imaged and photographed using Leica AM Meta Morph software (Molecular Devices, Sunnyvale, CA, US) at an excitation wavelength of 488 with a bandpass 510-nm emission filter. The cells were then alternately excited at 340 and 380 nm using a monochromator Policrome V (Till Photonics, Munich, Germany), and images of the fluorescent signals were captured each second through bandpass 510 nm filter using a CCD camera (Hamamatsu, Japan). All hardware was controlled, and Fura-2 images were analyzed using MetaFluor (Molecular Devices) software. To quantify differences in the amplitudes of Ca^{2+} transients, the ratio values were normalized using the formula $(DF)/F_0$ (referred to as norm. ratio). To compare multiple

samples (e.g., shShank3 and rescue results), ANOVA was used with Tukey's post-hoc tests. To analyze differences between two samples (e.g., Shank3-KO results) Student's two-tailed unpaired t-tests were used. Differences were considered statistically significant when $p < 0.05$.

Electrophysiology

Procedures were conducted in conformity with the European Communities Council Directive of November 1986 (86/609/ECC), in accordance with protocols approved by the Animal Care and Use Committee at the Universities of Perugia (Italy).

Mice were sacrificed by cervical dislocation and coronal corticostriatal slices (250 μm) were cut in Krebs' solution (in mM: 126 NaCl, 2.5 KCl, 1.2 $MgCl_2$, 1.2 NaH_2PO_4, 2.4 $CaCl_2$, 10 glucose, 25 $NaHCO_3$) using a vibratome. The slices were maintained in Kreb's solution, bubbled with a O_2 95% and CO_2 5% gas mixture at room temperature 27. A single slice was transferred to a recording chamber and submerged in a continuously flowing Kreb's solution (34°C, 2.5–3 ml/min) bubbled with a 95 % O_2–5 % CO_2 gas mixture. Whole-cell patch-clamp recordings were obtained from dorsolateral striatal neurons optically detected (Olympus) and electrophysiologically identified as MSNs 27. Whole-cell voltage-clamp (Vhold -80 mV) or current-clamp recordings were performed with borosilicate glass pipettes (4–7 MΩ; Ra 15–30 MΩ) filled with a standard internal solution containing (in mM): 125 K^+-gluconate, 0.1 $CaCl_2$, 2 $MgCl_2$, 0.1 EGTA, 10 HEPES, adjusted to pH 7.3 with KOH. Signals were amplified with a Multiclamp 700B amplifier (Molecular Devices), recorded and stored on PC using pClamp 10 (Molecular Devices). Membrane potentials and currents were recorded in the presence of 50 μM picrotoxin to block $GABA_A$ receptors. Glutamatergic excitatory postsynaptic currents (EPSCs) were evoked by a bipolar electrode connected to a stimulation unit (Grass Telefactor) and located in the white matter between the cortex and the striatum. Paired-pulse ratios of EPSC amplitudes (EPSC2/EPSC1) were obtained by a paired-pulse stimulation protocol at 50 ms inter-stimulus interval.

Drugs were bath-applied by switching the perfusion solution to drug-containing solution using a three-way tap syringe. Total replacement of the medium in the chamber occurred within 1 minute. CDPPB, CHPG, DHPG, NMDA, muscarine, picrotoxin, L-SOP, were purchased from Tocris-Cookson (Bristol, UK). CHPG, DHPG and muscarine were bath applied in the recording chamber alone and then co-applied with NMDA.

Data analysis was performed off-line using Clampfit 10 (Molecular Devices) and GraphPad Prism 5 (GraphPad Software). Values in the text and figures are mean ± SEM, n representing the number of recorded neurons. Student's *t*-test was used for statistical analysis with a significance level established at $p<0.05$.

Behavioral Assays

For behavioral analyses, 3-month-old age-matched littermate mice were used. All experimental procedures followed the guidelines established by the Italian Council on Animal Care and were approved by the Italian Government. All efforts were made to minimize the number of animals used and their suffering. *Shank-3*$^{-/-}$ mice and their littermates were housed in cages in groups of five with free access to food and water at 22°C

and with a 12-h alternating light/dark cycle. When obtaining behavioral profiles, the animals were tested once for each test. All tests were performed between 8 a.m. and 2 p.m.

Spontaneous motor activity—Motor function was evaluated in an activity cage (43 × 43 × 32 cm) (Ugo Basile, Varese, Italy) that was placed in a sound-attenuating room as previously described 28. The cage was fitted with two horizontal and vertical infrared beams that were located 2 cm and 4 cm from the floor of the cage, respectively. Before the start of the test each mouse was habituated to the testing room for 1 h. Cumulative horizontal and vertical movement counts were recorded for 10 min.

Repetitive self-grooming—Spontaneous repetitive self-grooming behavior was scored as previously described 29. Each mouse was individually placed into a standard cylinder, (46 cm length × 23.5 cm wide × 20 cm high). Cylinders were empty to eliminate digging in the bedding, which is a potentially competing behavior. The room was illuminated at ~ 40 lux. A front-mounted CC TV camera (Security Cameras Direct) was placed at ~ 1 m from the cages to record the sessions. Sessions were video-taped for 20 min. The first 10-min of habituation was not scored. Cumulative time spent grooming all the body regions during the second 10 min of the test session and the total number of grooming episodes was measured.

Spatial object recognition—Object location tests were performed in an arena according to the methods described in Kenney et al. 30, with slight modifications. Two visual cues were placed on two adjacent walls of an opaque white Plexiglas cage (58×50×43 cm) that was dimly lit from above (27 lux). The visual cues consisted of a black and white striped pattern (21×19.5 cm) that was affixed to the center of the northern wall and a black and gray checkered pattern (26.5×20 cm) that was placed in the center of the western wall. The objects were counterbalanced across locations. The cage and the objects were thoroughly wiped down with acetic acid (0.1%) before and after all behavioral procedures, which were observed and recorded using a camera mounted above the cage. Climbing or sitting on objects was not scored as object exploration. Mice that did not spend more than a total of 30 s exploring the objects during training or testing were excluded from the analysis. Mice were pre-exposed to the cage for 10 min. Twenty-four hours later, the mice were returned to the cage and allowed to explore two different objects placed in the NE and NW corners, and the time spent exploring the objects was recorded. Two hours later, the object the mouse had spent more time exploring in the previous session was moved to the SW corner of the cage (only this object was placed in the cage), and the mouse was allowed to re-explore the cage. Exploration was defined as a mouse having its nose directed toward the object and within approximately 1 cm of the object 31. Performance was evaluated by calculating a discrimination index (N-F/N+F), where N = the time spent exploring the moved object during T_2, and F = the time spent exploring the stationary object during T_2.

Sociability and Preference for Social Novelty Tests—The apparatus was a rectangular, three-chamber, transparent polycarbonate box (width = 42.5 cm, height = 22.2 cm, center chamber length = 17.8 cm, and side chamber lengths = 19.1 cm) as previously described 27. The test mouse was first placed in the middle compartment, and it was allowed to explore all three chambers for 10 min (habituation). Then, an unfamiliar adult DBA/2J

male mouse was placed in one side compartment. The opposite side compartment contained an empty wire cage. The social novelty tests were performed in the same apparatus immediately after sociability test. The cages were not cleaned between these two tests. For these tests, one side compartment contained the familiar mouse (from the previous sociability phase), while the other side contained an unfamiliar mouse. The new, unfamiliar mouse was placed in the wire cage that had been empty during the prior 10-min session. The familiar and unfamiliar animals were from different home cages and had never been in physical contact with the subject mouse or with each other. For both tests, the time spent in each chamber and the number of entries into each chamber were recorded for 10 min. The data were expressed as the difference in the scores between the time spent exploring the compartment containing the familiar mouse and the time spent in the empty compartment (for sociability tests) or the difference in the scores between the time spent containing the stranger animal and the time spent with the familiar mouse (for social novelty tests). An operator blind to the genotypes of the mice manually recorded the time spent in each chamber. We also evaluated a sociability index (SI) and a social novelty preference index (SNI) as follows: SI = (time exploring novel mouse 1 – time exploring novel object) / (time exploring novel mouse 1 + time exploring novel object) and SNI = (time exploring novel mouse 2 – time exploring familiar mouse) / (time exploring novel mouse 2 + time exploring familiar mouse).

Morris water maze test—The Morris water maze test was used to analyze changes in the learning and memory abilities of the mice according to the methods described in Morris 32 (adapted for mice). A circular water maze (120 cm in diameter x 50 cm in height) was used. A circular hidden platform with a diameter of 10 cm was placed inside the maze, and its surface was maintained at 0.5 cm below the surface of the water. Floating plastic particles were placed on the surface of the water to hide the platform from sight according to the methods of Zhang et al. 33. The temperature of the water was 25.0°C ± 0.5°C. For the habituation trials, the mice were placed in a random area inside the maze and allowed to swim for 60 sec. For the acquisition trials, the mice were submitted to 4 trials per day (with 60 sec inter-trial intervals) for 4 consecutive days during which each mouse was released into the pool at different starting points and trained to locate a constant platform position. At 24 hours after the last trial, a probe test was performed during which the platform was removed. Two days later, a reversal task was performed to assess cognitive flexibility. The platform was placed in the opposite quadrant of the tank, and 4 daily trials were performed for 4 days. On the fifth day, a probe trial was performed that was similar to that in the acquisition phase. The time spent in the target area and the latency to reaching the target zone were evaluated by an experimenter who was blind to the genotypes of the mice. After each trial, the mice were placed on a paper towel to dry, and they were then placed back into their home cages.

T-maze test—Mice were deprived of food until they reached 85–90% of their free-feeding body weight. They were habituated to a black wooden T-maze (with a 41-cm stem section and a 91-cm arms section). Each section was 11 cm wide and had walls that were 19 cm high. The mice were habituated to the T-maze and trained to obtain food within the maze for 5 days as previously described 28. During the acquisition phase, one arm was designated the

reinforcer (Coco Pops; Kellogg's) in each of ten daily trials. Each mouse was placed at the start of the maze and allowed to freely choose which arm to enter. The number of days required to reach the goal criterion (80% correct for 3 days) was recorded. Each mouse that met the goal for acquisition was then tested using a reversal procedure in which the reinforcer was switched to the opposite arm.

Pharmacological Treatment

CDPPB (Tocris) was dissolved in DMSO and polyethylene glycol 400 (DMSO:PEG 400 = 1:9) for the in vivo experiments and in DMSO only for the in vitro experiments. Wild-type and *Shank3Δ11-/-* mice received an intraperitoneal injection of the CDPPB (3 mg/kg)-containing solution or the same volume of a DSMO:PEG400 mixture 70 min before each behavioral test.

iPSC generation and differentiation into neurons

Fibroblasts obtained from patients diagnosed with Phenal-McDermid syndrome were collected according to a clinical protocol approved by the local Bioethical Committees of different medical centers. Participating individuals were informed of the objectives of the study and were required to sign an informed consent document before inclusion into the study. The deletion of 22q13.3 was confirmed in two of the PMS patients using genetic analysis. The detailed procedures used for the generation, maintenance, and characterization of iPS cells were previously described in 34. For immunofluorecence experiments were used the following primary antibodies: Nanog (Abcam cat. AB80892), Oct3/4 (Santa Cruz Biotechnology cat. sc-5279), Sox2 (Proteintech cat. 11064-1-AP), MAP2 (Abcam cat. AB11268), Synaptophysin (Sigma MS5768).

Data analysis

All of the behavioral, electrophysiological and imaging experiments and all data analyses were performed under blinded conditions in which the persons performing the experiment and the persons performing the analysis used a random numerical code, which was produced and known by another person, to label the differed samples.

Statistics

For all graphic data, *n* indicates number of biological replicates. The *n* values are reported in the Figure Legends and/or in the Results paragraph describing the experiments. All quantitative biochemical data are representative of three independent experiments, and all behavioral data are representative of at least two experiments. The sample size for biochemical, morphological Ca^{2+} imaging and electrophysiological experiments was determined by empirical evidence accumulated in our laboratory and also on previous literature. For behavioral test the number of mice was chosen to ensure adequate power a on the basis of the program G*power 3.1 (Charan et al., J Pharmacol Pharmacother 4(4): 303-306, 2013), available on line : http://www.gpower.hhu.de/.

Based on the number of comparisons and the pattern of data distribution, appropriate statistical tests were used to analyze the data. Unpaired two-tailed *t*-test was used to evaluate the difference between two groups; the variances in two groups were similar in all data sets.

Two-way analysis of variance followed by *post hoc* test was used for comparison of multiple samples. Significance was set at $P<0.05$. All values are presented as mean ± SEM.

Results

Deletion of Shank3 in mice results in ASD-like behavior

To determine whether a Shank3 mutation in mice results in ASD-like behavior and ID, we characterized the behavior of *Shank3Δ11*$^{-/-}$ mice (previously called *ProSAP2/Shank3αβ*$^{-/-}$ in 25).

To analyze repetitive, stereotyped behavior, which is one of the two cores symptoms of ASD, we measured grooming behaviors. In KO mice, we detected an increase in self-grooming activity in terms of the time spent grooming and the number of grooming episodes (Figure 1A).

Given that impaired social interaction is the second core symptom of ASD, we tested sociability in *Shank3Δ11*$^{-/-}$ mice using a three-chamber test (Figure 1B). We observed that KO mice were impaired in that they spent more time exploring the compartment containing the empty cage than the compartment containing the stranger mouse (left panel). In addition, KO mice remained closer to the familiar stranger for longer period of time, which suggests impaired social recognition (right panel). Accordingly, the corresponding sociability index (SI) and the social novelty preference index (SNI) scores were lower in the KO mice than in their littermates. Because *SHANK3* mutations are often associated with ID, we tested spatial learning and memory in *Shank3Δ11*$^{-/-}$ mice. To evaluate spatial memory, we used a spatial object recognition test in which we analyzed a discrimination index with an inter-trial interval of 120 min. We did not detect significant differences between the two genotypes in this test (Figure 1C).

We also tested the mice in a water-maze place navigation task. KO mice showed normal acquisition compared to their littermates (Figure 1D left panel). Spatial memory was then tested using a probe trial, which was administered after a 4-day training period during which we measured the latency (Figure 1D, center panel) and the time required to reach the target quadrant (Figure 1D, right panel). We did not detect any significant difference between the genotypes. The latency and the percentage of time spent swimming to the target quadrant were also not significantly different. On the contrary, the escape latency of KO mice was longer than the latency in WT mice on day 8 and day 9 (Figure1E, left panel). In the probe trial, the KO mice took longer to find the target zone (Figure 1E, center panel) and spent less time than WT mice to swim to the quadrant that previously housed the platform (Figure1E, right panel). *Shank3Δ11*$^{-/-}$ mice also showed impairments in the T-maze task, but only during the reversal phase (Figure1F). KO mice required more days to achieve the criterion than WT mice. This resistance to change in a learned pattern of behavior indicates that *Shank3Δ11*$^{-/-}$ mice recapitulate cognitive rigidity, which is a typical symptom of many neuropsychiatric disorders, including ASD.

We next analyzed behaviors related to avoidance of inanimate objects and restricted interests. In the marble burying test, KO mice buried fewer marbles than WT mice and took

a larger amount of time to bury the first marble (Supplementary Figure 1A). We detected a similar pattern in avoidance behavior when we measured nest building in that KO mice had lower nest building scores than WT mice (Supplementary Figure 1B). The corresponding AUC (Supplementary Figure 1C) was significantly lower in KO mice than in WT mice. These results strongly suggest that *Shank3Δ11*$^{-/-}$ mice exhibit restricted interest and an avoidance phenotype when exposed to inanimate objects.

We next characterized motor coordination and motor learning, behaviors that are also often altered in ASD patients, in *Shank3Δ11*$^{-/-}$ mice. Fine motor coordination and balance were assessed using the beam walking assay. We did not observe any difference in the mean time required to cross to the escape box between the two genotypes (Supplementary Figure 1D). On the contrary, during the pole test, KO mice took longer to complete the task than WT mice (Supplementary Figure 1E) and they had more difficulty in remaining suspended from the lid during the hanging wire test (Supplementary Figure 1F). In rotarod tests, KO mice showed a defect only in the fourth trial of the first day of evaluation (Supplementary Figure 1G). These data indicate that *Shank3Δ11*$^{-/-}$ mice exhibit only minor deficits in motor coordination.

Because there is a strong association between anxiety and autism, we also tested *Shank3Δ11*$^{-/-}$ mice using an elevated plus maze, but we did not find any differences between WT and KO animals (Supplementary Figure 1H).

Associated symptoms, which have also been documented in a subset of individuals with ASD, include increased aggression and hyposensitivity to pain. Indeed, we found that aggressive behavior was significantly increased in KO mice compared to WT mice (Supplementary Figure 1I) and that KO mice showed a higher mean threshold latency than WT mice in hot plate tests (Supplementary Figure 1L).

Interestingly, we also tested *Shank3Δ1*$^{+/-}$ mice, and we did not observe any major behavioral impairment except for a longer time to complete the pole test than was observed in WT mice (Supplementary Table 1).

Shank3 absence alters the synaptic localization of Homer and the mGlu5 receptor

Based on our previous results that showed that knock-down of Shank3 in primary neuronal cultures caused a significant reduction in the mGlu5 receptor 14, we measured mGlu5 and Homer1b/c protein levels in total homogenates and PSD fractions from the striatum, cortex and hippocampus of *Shank3Δ11*$^{-/-}$ mice.

In PSD fractions obtained from KO animals, we observed a reduction in Homer1b/c protein levels in the striatum, a reduction in both mGlu5 and Homer1b/c in the cortex, and no change in mGlu5 and Homer1b/c levels in the hippocampus (Figure 2A). Interestingly, decreased mGlu5 receptor and Homer1b/c levels were detected only in the PSD fractions, and there was no significant change in the level of either protein in total homogenates (Supplementary Figure 2A). These biochemical data indicate that *in vivo*, Shank3 absence alters mGlu5 receptor and Homer 1b/c protein expression only in the PSD of specific brain regions.

To understand whether the localization of Homer was altered in the absence of Shank3, we next analyzed postsynaptic Homer1 signals in the dorsal striatum, in layers 2-3 of the primary somatosensory cortex and in the CA1 stratum radiatum of the hippocampus in *Shank3Δ11*$^{-/-}$ mice using immunofluorescence and confocal microscopy. First, we found that the density of Homer1-positive puncta was unchanged between WT and *Shank3Δ11*$^{-/-}$ mice in all three brains regions (Figure 2B and Supplementary Figure 2B). Interestingly, KO mice showed an increase in the density of Homer1 puncta that did not colocalize with PSD-95 and, in parallel, a robust reduction in double-labeled puncta in both the dorsal striatum and the somatosensory cortex (Figure 2B and Supplementary Figure 2B). In contrast, we did not observe any change in Homer1 localization in the CA1 area of the hippocampus in KO mice (Figure 2B and Supplementary Figure 2B).

We then examined whether these alterations in the synaptic localization of Homer1 compromised the interaction between Homer and the mGlu5 receptor by performing co-immunoprecipitation assays using tissues from the striatum, cortex and hippocampus.

Quantitative analysis using WB was performed to co-immunoprecipitate mGlu5 using Homer1b/c antibodies. The results revealed a significant reduction in protein-protein interactions between mGlu5 and Homer1b/c in both the striatum and the cortex, but not in the hippocampus, in *Shank3Δ11*$^{-/-}$ mice compared to WT mice (Figure 2C). We also co-immunoprecipitated SynGAP and GluN2A using PSD-95 antibodies in the striatum, cortex and hippocampus of *Shank3Δ11*$^{-/-}$ and WT mice. Quantitative analysis of corresponding blots showed that there was no difference in the interaction between PSD-95 and SynGAP or PSD-95 and GluN2A between *Shank3Δ11*$^{-/-}$ and WT mice in any the brain areas analyzed. These results confirm that the absence of Shank3 specifically reduced mGlu5/Homer interactions in the striatum and cortex (Supplementary Figure 2C).

Finally, in consideration for the results obtained in the different brain areas, we next sought to determine whether Shank3 levels were different in the striatum, cortex and hippocampus in total homogenates and PSD fractions, and we found that its expression was lower in the hippocampus (Supplementary Figure 2D)

Taken together, these data suggest that the absence of Shank3 causes brain region-specific alterations in both protein levels and the localization of the mGlu5 receptor and Homer1b/c at synapses and that these changes prevent the normal formation of the mGlu5/Homer complex, which is essential to mediating mGlu5 intracellular signaling35–37.

To clarify whether Homer1b/c localization was altered also in neurons derived from patients with PMS who exhibited *SHANK3* haploinsufficiency, we established human induced pluripotent stem cell (hiPSC) lines using cells derived from two different patients with PMS, one of whom had a deletion of approximately 7.99 Mb (Patient 1) and one of whom had a deletion that was 22q13.3 ARSA-negative (Patient 2). As a control, we used hiPSCs that were generated from two healthy donors. The control and PMS clones were tested to determine the expression of endogenous pluripotency markers (Supplementary Figure 3A-B). The hiPSC clones were differentiated into cortical neurons via the generation of neural-rosette intermediate neural progenitors, and they were subsequently differentiated for 80

days. We confirmed using WB that there was a reduction in Shank3 protein levels in the neurons obtained from both of the PMS patients compared to the Shank3 levels in the control (Supplementary Figure 3C). To analyze Homer cluster localization, we infected neuronal progenitors with a lentivirus expressing Homer-GFP. Interestingly, after 80 days of differentiation, we observed a significant reduction in the number of Homer puncta that co-localized with Synaptophysin in neurons derived from both of the PMS patients compared to the co-localization observed in the neurons derived from the controls (Figure 2D). These results suggest that in human neurons, Shank3 is essential for Homer1b/c synaptic localization.

Shank3 absence impairs the mGlu5-mediated intracellular release of calcium

Shank/Homer1b/c protein interactions play a major role in mediating mGlu5 intracellular signaling by linking the mGlu5 receptor to IP_3 receptors (IP_3Rs) 10, 15–17, 38–41.

We therefore investigated whether elimination of Shank3 altered the generation of mGlu5 receptor-mediated Ca^{2+} signals in cortical neurons isolated from *Shank3Δ11*$^{-/-}$ mice. First, we confirmed that the reduction in the mGlu5 receptor and Homer1b/c protein levels that was observed in the cortex was also observed in the synaptic fractions of cultured cortical neurons obtained from *Shank3Δ11*$^{-/-}$ mice (Figure 3A). Then, we measured the induction of Ca^{2+} transients by 200 μM DHPG, a specific group I metabotropic receptor agonist. Figure 3B shows that DHPG-induced Ca^{2+} transients in KO neurons were significantly lower than in WT neurons, indicating that the elimination of the Shank3 protein impaired mGlu5-mediated signaling in cortical neurons. To confirm that these alterations in calcium signaling mediated by mGlu5 receptor activation were due to alterations in the synaptic distribution of Homer, we analyzed the synaptic localization of Homer1b/c using immunofluorescence in cultured cortical neurons that were derived from *Shank3Δ11*$^{-/-}$ and WT mice. Quantification of the co-localization of Homer puncta and Bassoon revealed that the postsynaptic localization of Homer was reduced in the *Shank3Δ11*$^{-/-}$ cortical cultured neurons (Figure 3C).

In a second series of experiments, we knocked down Shank3 using specific shRNA sequences. Supplementary Figure 4A–B shows that the administration of 200 μM DHPG elicited a much lower Ca^{2+} transient in shRNA-Shank3-tranfected neurons than in control neurons (either non-transfected or transfected with a GFP-expressing plasmid) (Supplementary Figure 4A-B). When the shShank3-resistant form of Shank3 was co-expressed with the shRNA-Shank3 plasmid, the DHPG-induced Ca^{2+} transients were restored to control levels, indicating that the effect of shRNA-Shank3 transfection was specific. We also confirmed using immunofluorescence that Homer-Bassoon co-localization was altered in Shank3 knock-down neurons (Supplementary Figure 4C).

Our previous results suggested that *in vitro*, the reduction in mGlu5 receptor activity that was caused by Shank3 knock-down could be rescued using CDPPB, a positive allosteric modulator of mGlu5 receptor 14, 42. For these experiments, DIV12-14 cortical neuronal cultures were loaded with Fura-2 and challenged with 200 μM DHPG in either the presence (5 min of preincubation, Figure 3D) or the absence of 3 μM CDPPB. As expected, in the Shank3Δ11$^{-/-}$ cortical neurons, the DHPG-induced Ca2+ transients were approximately 40%

lower than in the WT neurons. After preincubation with CDPPB, the Ca^{2+} transients in the Shank3Δ11$^{-/-}$ neurons were significantly augmented, reaching the level of WT neurons (Figure 3D).

The effect of mGlu5 stimulation on NMDA responses in striatal medium spiny neurons is dependent on Shank3

Because we observed a disruption in synaptic Homer localization in the absence of Shank3 and high expression of Shank3 in the striatum, we tested the electrophysiological properties of striatal neurons.

Patch-clamp recordings were obtained using medium spiny neurons (MSNs) obtained from WT and KO mice to explore whether the deletion of Shank3 affected the basal membrane properties of striatal neurons. Current-voltage curves were obtained by delivering hyperpolarizing and depolarizing steps of currents to the MSNs of KO (n=6) and WT (n=6) mice, and we observed no difference between these two groups of neurons, suggesting that the basal membrane properties of MSNs do not depend on Shank3 expression (Figure 4 A-B).

We subsequently studied whether Shank3 was responsible for the observed changes in the membrane potential and the ionic currents induced by the stimulation of group I mGlu receptors in MSNs. Activation of these types of metabotropic glutamate receptors has been shown to enhance the membrane depolarization/inward current that is produced by the activation of the NMDA receptor in striatal MSNs 43. As shown in Figures 4C and 4G, the application of 30 μM NMDA produced a membrane depolarization of approximately 15 mV and an inward current of approximately -70 pA in MSNs in WT mice, while the co-application of NMDA in the presence of DHPG produced a significantly larger depolarization (Figure 4C-D) and inward current (Figure 4 G-H). Interestingly, in the MSNs obtained from KO mice, the co-application of NMDA plus DHPG failed to produce a membrane depolarization and inward current that was larger than those observed in the presence of NMDA alone (Fig. 4E-H).

Because mGlu5 receptors are mainly involved in potentiation of NMDA responses in striatal MSNs 44, we also tested whether the selective mGlu5 receptor agonist CHPG would be able to increase NMDA receptor-mediated responses in MSNs obtained from WT and KO mice.

As shown in Supplementary Figure 4A-B, when 500 μM CHPG was applied for 5 minutes, it significantly enhanced the NMDA receptor-mediated membrane depolarization of MSNs (n=5) obtained from WT mice, but it failed to produce a larger NMDA response in the MSNs obtained from KO animals (n=5). Taken together, these data confirm that in striatal MSNs, normal NMDA receptor function depends on mGlu5 receptor activity, and this interplay is essentially disrupted by the deletion of Shank3.

We also explored whether Shank3 is involved in the functions of a different class of metabotropic receptors, the muscarinic cholinergic receptors. Because in MSNs, the NMDA receptor-mediated response is increased by the activation of muscarinic cholinergic receptors 43, we tested whether Shank3 also plays a role in this process (Supplementary Figure 4C-

Europe PMC Funders Author Manuscripts

D). Interestingly, we found that activating cholinergic receptors using muscarine increased NMDA-mediated neuronal depolarization in MSNs obtained from both WT and KO mice. These experiments confirm that Shank3 does not play a major role in mediating metabotropic responses that are related to the activation of cholinergic receptors in MSNs.

Finally, we tested whether Shank3 was involved in the function of presynaptic group III mGlu receptors. In fact, stimulating mGluIII receptors is known to inhibit glutamate release and excitatory postsynaptic currents (EPSCs) in MSNs via a presynaptic mechanism of action. Thus, we first tested the effect of applying a 10 μM solution of the mGlu III receptor agonist L-SOP to MSNs for 10 minutes. We found that the EPSC amplitude was reduced by 34.72 ± 8.2% ($n=4$, $p<0.05$) and 47.9 ±5.9% ($n=6$, $p<0.05$) in WT and KO mice, respectively (Supplementary Figure 4E-F). Moreover, we measured the effect of L-SOP on paired-pulse facilitation (PPF) because changes in PPF are indicative of a presynaptic mechanism of action. As shown in Supplementary Figure 4F, PPF ($EPSC_2/EPSC_1$) was significantly increased in MSNs obtained from both WT and KO animals in the presence of L-SOP. These results substantiate the hypothesis that Shank3 deletion specifically affects mGlu5 signaling in striatal MSNs.

We then tested the effect of CDPPB on MSNs obtained from WT and KO mice, and as shown in Figures 4I-J, CDPPB treatment was able to recover normal NMDA receptor functions, which depend on mGlu5 receptor activity, in the MSNs obtained from Shank3 KO mice to levels comparable to those in the MSNs obtained from WT mice.

Surprisingly, we found that, in Shank3 KO MSN, CDPPB alone was able to rescue the activation of NMDA receptor mediated responses; on the contrary, in culture cortical neurons from Shank3 KO mice, CDPPB alone was not able to rescue the impaired calcium release (data not shown). Thus we cannot exclude neither that in MSN CDPPB has also a partial intrinsic agonist activity nor that in striatal slices preparation the glutamate tone is higher then in cultured neuronal preparation and it is enough to partially activate mGlu5.

The mGlu5 receptor positive agonist CDPPB rescues ASD-like behavior in *Shank3Δ11*$^{-/-}$ mice

Because CDPPB was able to rescue the functional defects observed in both cortical and striatal neurons, we tested whether the behavioral abnormalities observed in *Shank3Δ11*$^{-/-}$ mice could be pharmacologically ameliorated by treating KO mice with CDPPB 45, 46.

The behavioral profiles of KO mice were evaluated after treatment with CDPPB (3 mg/kg i.p.) or vehicle (veh), which was administered acutely or repeatedly 70 min before each test. The results are reported in Figure 5. The increased self-grooming activity observed in KO mice was reduced by acute treatment with CDPPB (Figure 5B). There was also a significant reduction in the mean number of grooming episodes. Notably, the drug did not affect motor activity when mice were evaluated immediately after self-grooming activity (Figure 5A). Reduced sociability (Figure 5C, left) was slightly, but not significantly, rescued in KO animals by acute treatment with CDPPB when analyzed as time spent close to the stranger/object. However, the SI, which measures sniffing activity, was significantly increased when the animals were given CDPPB. Social recognition was completely rescued in *Shank3Δ11-/-*

mice, when analyzed as either the time spent close to the stranger2/stranger1 or sniffing activity (Figure 5C, right). In the water-maze place navigation task (Figure 5D), the KO mice showed normal acquisition compared to WT mice in terms of mean time required to reach the platform. A significant latency reduction between the first and the fourth trial was observed in all groups (Figure 5D, left panel), suggesting a normal progression of learning. During the probe test, no difference among the groups was shown in latency (Figure 5D, center panel) or the time spent in the target zone (Figure 5D, right panel). During reversal (Figure 5E), a significant difference in the escape latency across the trials was observed. KO mice treated with vehicle were completely impaired compared to their littermates, while CDPPB reduced escape latency during the learning phase (Figure 5E, left panel).

When submitted to the probe trial on day 10, the KO mice that were treated with CDPPB required less time to find the target zone (Figure 5E, center panel) and spent more time than the KO mice treated with vehicle to swim to the quadrant that previously housed the platform (Figure 5E, right panel).

All of these pharmacological data demonstrate that the positive allosteric modulation of the mGlu5 receptor was able to rescue the behavioral deficits observed in the *Shank3Δ11*$^{-/-}$ mice that resulted from altered mGlu5 signaling.

Discussion

To evaluate the role of Shank3 in synapse function and to develop therapies that might ameliorate or even reverse the neuropsychiatric symptoms experienced by patients with PMS or other mutations in the *SHANK3* gene, we characterized the behavioral, molecular and electrophysiological phenotypes of *Shank3* mutant mice that were generated by deleting exon 11 25. Among the *Shank3* mutants that were available, *Shank3Δ11*$^{-/-}$ mice are less often studied, although they are highly homologous to the *Shank3B*$^{-/-}$ mutants described by Peça et al., 4.

Behaviorally, our analysis demonstrates that the *Shank3Δ11*$^{-/-}$ mutant is an excellent model for studying the role of Shank3 in the pathogenesis of PMS and ASD. Indeed, this mutant line shows repetitive and stereotyped behavior, restricted interests and impaired social interactions, which are the core diagnostic features of ASD and are similar to the features observed in most other Shank3 KO mice (see Figure 1). In addition, our mice, similar to the Shank3D4-9-/- mice, displayed impairments in the reversal phase of the Morris Water maze and T-maze tests 3–7, 25, 47–49. Because PMS patients are heterozygous for Shank3 mutations/deletions, we also tested all of the behavioral tasks in *Shank3Δ11*$^{-/+}$ mice, but we did not find any significant behavioral defects in the heterozygous mice. Our results are in line with the results described in the majority of studies that have been performed using other Shank3 KO mice, in which it has been demonstrated that behavioral alterations are present only in Shank3 KO mice. It is possible that there are unknown compensatory mechanisms that reduce the severity of the Shank3 deletion in the heterozygous mice.

The results of our molecular studies further indicate that Shank3 plays a major role in modulating mGlu5 signaling by regulating Homer recruitment/localization to the PSD in brain regions that are highly associated with ASD-like behavior 50–52.

Finally, our findings demonstrate that treatment with a PAM for mGlu5 rescued both the functional and the behavioral defects observed in the *Shank3Δ11*$^{-/-}$ mutants.

Deletion of Shank3 alters the recruitment of Homer to the PSD in the cortex and striatum

Shank proteins are indirectly connected to group I mGlu receptors by Homer proteins, which contain coiled-coil domains. For Shank1, it has already been demonstrated that the Shank/Homer complex regulates their reciprocal localization at the PSD 11, 38. The biochemical and morphological data in this study demonstrate that in *Shank3Δ11*$^{-/-}$ mice, the localization of Homer1b/c to the PSD is significantly reduced in both striatal and cortical neurons. As consequence, the synaptic association of Homer1b/c and mGlu5 in these two areas is reduced (see Figure 2).

Biochemical analysis of synaptosome preparations from the cortex, hippocampus and striatum of *Shank3Δ11*$^{-/-}$ mice have already shown that there is a significant increase in GluN2B in the hippocampus and a slight reduction in various AMPA receptor subunits in all of the regions analyzed 25. Here we specifically investigated mGlu5 and Homer protein levels based on our previous work showing a reduction in the expression of mGlu5 in Shank3 knock-down neurons 14. Importantly, both mGlu5 and Homer1b/c were reduced in the PSD fractions obtained from the cortex and striatum of *Shank3Δ11*$^{-/-}$ mice, while their expression in hippocampus was unaffected.

Thus, our data indicate that depending on the brain region, Shank3 performs different functions at synapses. Even if the underlying molecular mechanism is not yet clear, biochemical analyses in several other *Shank3* mutant mice have suggested that the brain region-specific function of Shank3 in regulating glutamate receptor levels at synapses might further depend on the different splice variants that are expressed. For example, *Shank3B*$^{-/-}$ mutants exhibited a major reduction in GluA2, GluN2A and GluN2B in striatal PSDs 4 and *Shank3*$^{e4-9}$ mutants exhibited a reduction in GluA1 in whole forebrain PSDs 3, 5. These alterations were not evaluated in *Shank3Δ11*$^{-/-}$ and *Shank3*$^{\Delta C/\Delta C}$ mice. In contrast, *Shank3*$^{\Delta C/\Delta C}$ mice showed a strong increase in mGlu5 in hippocampal PSD preparations 7. A common alteration observed in several Shank3 mutants is a reduction in Homer, as has been observed in forebrain PSDs of *Shank3*$^{e4-9}$ 5 mutants and in the striatal PSDs of *Shank3B*$^{-/-}$ mutants 4.

However, a systematic molecular analysis of each brain region of interest and how it is correlated to the regional expression level of all three Shank proteins and their isoforms alike has yet to be performed to decipher the defects in the highly complex synaptic transmission identified in *Shank* mutants. Finally, Homer1b/c synaptic localization is strongly impaired in hiPSC-derived neurons that were obtained from patients with PMS who exhibited SHANK3 haploinsufficiency, suggesting that Shank3 is also important for the normal clustering of Homer1b/c into synaptic puncta in human neurons (Figure 2D).

Deletion of Shank3 alters mGlu5 function in cortex and striatum, but not in hippocampus

Because mGluR-Homer complex formation is required for the correct function of mGluRs 53, we have provided *in vitro* data showing that mGlu5-dependent Ca^{2+} release from intracellular stores is impaired in cortical neurons in *Shank3Δ11*$^{-/-}$ mice (Figure 3B). We also provide *in vivo* data showing that mGlu5-dependent NMDA receptor potentiation is completely abolished in striatal neurons obtained from *Shank3Δ11*$^{-/-}$ mice (Figure 4). To the contrary, we did not observe any defects in DHPG-mediated LTD in the hippocampus in *Shank3Δ11*$^{-/-}$ mice (Supplementary Figure 6). The function of Shank3 in regulating mGlu5 signaling is specifically supported by the following data sets: 1) The expression of shRNA-resistant Shank3 rescued the changes in DHPG-induced Ca^{2+} release from intracellular stores observed in Shank3 knock-down cortical neurons (Supplementary Figure 4A-B); 2) Shank3 does not play a major role in mediating metabotropic responses related to the activation of cholinergic receptors in MSNs and is not involved in the regulation of presynaptic group III mGluRs (Supplementary Figure 5); 3) CDPPB induced the positive modulation of mGlu5 activity and rescued the functional defects observed in both cortical and striatal neurons in *Shank3Δ11*$^{-/-}$ mice to WT levels (Figure 3D and Figure 4I-J)

These results suggest that altered group I mGluR signaling could be one of the most common impaired synaptic signaling pathways in the *Shank3* mutant brain.

ASD-like behaviors were reversed in Shank3 mutant mice by an mGlu5 PAM

Our data are in line with recent evidence linking Homer proteins to mGlu5 receptor-mediated synaptic plasticity and ASD 21. Indeed, inhibiting mGlu5-Homer complex formation impaired mGluR-dependent LTD and protein synthesis in normal mice 53, while in a mouse model of Fragile-X syndrome (FXS), mGlu5 receptors were less associated with Homer1b/c and more associated with Homer1a 20, 53, resulting in alterations in the cross-linking activity of Homer1b/c 38. Similarly, in a mouse model of Angelman Syndrome, mGlu5 receptor-dependent synaptic plasticity was altered because it showed an increased association with Homer 1b/c 54. However, in these two mouse models, an enhancement in hippocampal mGlu5 receptor function was the core phenotype 53, 54, which was contrary to the decrease in mGlu5 receptor function we observed in *Shank3Δ11*$^{-/-}$ mutants. This indicates that changes in the function of synapses might occur if mGlu5 signaling is pathologically modified in any direction. Interestingly, Homer1 itself has recently been identified as a novel risk gene for non-syndromic ASD 55, and another study showed that mGlu5 gene expression was reduced in the dorsolateral prefrontal cortex (DLPFC) in ASD patients 19.

Our previous findings prompted us to test whether the ASD-like behaviors of *Shank3Δ11*$^{-/-}$ mutants could be reversed by the application of an allosteric mGlu5 agonist, such as CDPPB. Indeed, we found that repetitive and stereotyped behavior, a lack of cognitive flexibility and partially impaired social interactions were rescued by *in vivo* treatment with CDPPB (Figure 5). A similar approach was used to rescue behavioral phenotypes in a *Shank2* mutant line 56. Importantly, the potential of positive allosteric mGlu5 modulation has already been tested in other models of ASD. In particular, Auerbach et al. demonstrated that treatment with CDPPB restored synaptic and behavioral deficits in *Tsc2*$^{+/-}$ mutant mice

57, and very recently, Lin et al. showed that the systemic administration of CDPPB ameliorated the behavioral defects observed in Sarm1 knockdown mice 58. Our data, including our observation that there were no alterations in mGlu5 signaling in the hippocampus, suggest that the ASD-like behavioral defects that are the result of mGlu5 signaling impairments in the striatum and cortex of *Shank3Δ11*$^{-/-}$ mice can be functional rescued by CDPPB, even if we cannot totally exclude the possibility that CDPPB might have an effect on other brain areas.

Our results confirm that positive allosteric modulation of mGlu5 antagonizes ASD-like behaviors and suggest that mGlu5 activity could be viewed as a potential therapeutic target for neurodevelopmental disorders in general, as has been suggested by many recent studies 59. Therefore, our findings open up new possibilities for the pharmacological treatment of patients affected by PMS and *SHANK3* mutations.

Supplementary Material

Refer to Web version on PubMed Central for supplementary material.

Acknowledgements

This work was supported by the Comitato Telethon Fondazione Onlus (grant no. GGP13187 to C.S. and GGP11095 to C.S. and M.G.), Italian Institute of Technology (Seed Grant to C.S.), Foundation Jérôme Lejeune (to C.V.) and the Fondazione CARIPLO (project number 2012-0593 to C.S. and 2013-0879 to C.V.). TMB received support from the Innovative Medicines Initiative Joint Undertaking under grant agreement number 115300, the resources of which are composed of a financial contribution from the European Union's Seventh Framework Programme (FP7/2007-2013) and a generous contribution from the EFPIA companies. MJS was supported by Baustein 3.2 of Ulm University (L.SBN.0081) and by the DAAD (PROCOPE 57049403).

References

1. Phelan K, McDermid HE. The 22q13.3 Deletion Syndrome (Phelan-McDermid Syndrome). Mol Syndromol. 2012; 2(3-5):186–201. [PubMed: 22670140]
2. Durand CM, Betancur C, Boeckers TM, Bockmann J, Chaste P, Fauchereau F, et al. Mutations in the gene encoding the synaptic scaffolding protein SHANK3 are associated with autism spectrum disorders. Nat Genet. 2007; 39(1):25–27. [PubMed: 17173049]
3. Bozdagi O, Sakurai T, Papapetrou D, Wang X, Dickstein DL, Takahashi N, et al. Haploinsufficiency of the autism-associated Shank3 gene leads to deficits in synaptic function, social interaction, and social communication. Mol Autism. 2010; 1(1):15. [PubMed: 21167025]
4. Peça J, Feliciano C, Ting JT, Wang W, Wells MF, Venkatraman TN, et al. Shank3 mutant mice display autistic-like behaviours and striatal dysfunction. Nature. 2011; 472(7344):437–442. [PubMed: 21423165]
5. Wang X, McCoy PA, Rodriguiz RM, Pan Y, Je HS, Roberts AC, et al. Synaptic dysfunction and abnormal behaviors in mice lacking major isoforms of Shank3. Hum Mol Genet. 2011; 20(15): 3093–3108. [PubMed: 21558424]
6. Yang M, Bozdagi O, Scattoni ML, Wöhr M, Roullet FI, Katz AM, et al. Reduced excitatory neurotransmission and mild autism-relevant phenotypes in adolescent Shank3 null mutant mice. J Neurosci. 2012; 32(19):6525–6541. [PubMed: 22573675]
7. Kouser M, Speed HE, Dewey CM, Reimers JM, Widman AJ, Gupta N, et al. Loss of predominant Shank3 isoforms results in hippocampus-dependent impairments in behavior and synaptic transmission. J Neurosci. 2013; 33(47):18448–18468. [PubMed: 24259569]
8. Speed HE, Kouser M, Xuan Z, Reimers JM, Ochoa CF, Gupta N, et al. Autism-Associated Insertion Mutation (InsG) of Shank3 Exon 21 Causes Impaired Synaptic Transmission and Behavioral Deficits. J Neurosci. 2015; 35(26):9648–9665. [PubMed: 26134648]

9. Jiang YH, Ehlers MD. Modeling autism by SHANK gene mutations in mice. Neuron. 2013; 78(1): 8–27. [PubMed: 23583105]
10. Sala C, Roussignol G, Meldolesi J, Fagni L. Key role of the postsynaptic density scaffold proteins shank and homer in the functional architecture of Ca2+ homeostasis at dendritic spines in hippocampal neurons. Journal of Neuroscience. 2005; 25(18):4587–4592. [PubMed: 15872106]
11. Sala C, Piech V, Wilson NR, Passafaro M, Liu GS, Sheng M. Regulation of dendritic spine morphology and synaptic function by Shank and Homer. Neuron. 2001; 31(1):115–130. [PubMed: 11498055]
12. Hung AY, Futai K, Sala C, Valtschanoff JG, Ryu J, Woodworth MA, et al. Smaller dendritic spines, weaker synaptic transmission, but enhanced spatial learning in mice lacking Shank1. J Neurosci. 2008; 28(7):1697–1708. [PubMed: 18272690]
13. Roussignol G, Ango F, Romorini S, Tu JC, Sala C, Worley PF, et al. Shank expression is sufficient to induce functional dendritic spine synapses in aspiny neurons. Journal of Neuroscience. 2005; 25(14):3560–3570. [PubMed: 15814786]
14. Verpelli C, Dvoretskova E, Vicidomini C, Rossi F, Chiappalone M, Schoen M, et al. Importance of Shank3 protein in regulating metabotropic glutamate receptor 5 (mGluR5) expression and signaling at synapses. J Biol Chem. 2011; 286(40):34839–34850. [PubMed: 21795692]
15. Naisbitt S, Kim E, Tu JC, Xiao B, Sala C, Valtschanoff J, et al. Shank, a novel family of postsynaptic density proteins that binds to the NMDA receptor/PSD-95/GKAP complex and cortactin. Neuron. 1999; 23(3):569–582. [PubMed: 10433268]
16. Tu JC, Xiao B, Naisbitt S, Yuan JP, Petralia RS, Brakeman P, et al. Coupling of mGluR/Homer and PSD-95 complexes by the Shank family of postsynaptic density proteins. Neuron. 1999; 23(3): 583–592. [PubMed: 10433269]
17. Boeckers TM, Kreutz MR, Winter C, Zuschratter W, Smalla KH, Sanmarti-Vila L, et al. Proline-rich synapse-associated protein-1/cortactin binding protein 1 (ProSAP1/CortBP1) is a PDZ-domain protein highly enriched in the postsynaptic density. J Neurosci. 1999; 19(15):6506–6518. [PubMed: 10414979]
18. Boeckers TM, winter C, Smalla KH, Kreutz MR, Bockmann J, Seidenbecher C, et al. Proline-rich synapse-associated proteins ProSAP1 and ProSAP2 interact with synaptic proteins of the SAPAP/GKAP family. Biochem Biophys Res Commun. 1999; 264(1):247–252. [PubMed: 10527873]
19. Chana G, Laskaris L, Pantelis C, Gillett P, Testa R, Zantomio D, et al. Decreased expression of mGluR5 within the dorsolateral prefrontal cortex in autism and increased microglial number in mGluR5 knockout mice: Pathophysiological and neurobehavioral implications. Brain Behav Immun. 2015
20. Giuffrida R, Musumeci S, D'Antoni S, Bonaccorso CM, Giuffrida-Stella AM, Oostra BA, et al. A reduced number of metabotropic glutamate subtype 5 receptors are associated with constitutive homer proteins in a mouse model of fragile X syndrome. J Neurosci. 2005; 25(39):8908–8916. [PubMed: 16192381]
21. Ronesi JA, Huber KM. Homer interactions are necessary for metabotropic glutamate receptor-induced long-term depression and translational activation. J Neurosci. 2008; 28(2):543–547. [PubMed: 18184796]
22. Lujan R, Roberts JD, Shigemoto R, Ohishi H, Somogyi P. Differential plasma membrane distribution of metabotropic glutamate receptors mGluR1 alpha, mGluR2 and mGluR5, relative to neurotransmitter release sites. J Chem Neuroanat. 1997; 13:219–241. [PubMed: 9412905]
23. Shigemoto R, Nomura S, Ohishi H, Sugihara H, Nakanishi S, Mizuno N. Immunohistochemical localization of a metabotropic glutamate receptor, mGluR5, in the rat brain. Neurosci Lett. 1993; 163(1):53–57. [PubMed: 8295733]
24. Romano C, Sesma MA, McDonald CT, O'Malley K, Van den Pol AN, Olney JW. Distribution of metabotropic glutamate receptor mGluR5 immunoreactivity in rat brain. J Comp Neurol. 1995; 355(3):455–469. [PubMed: 7636025]
25. Schmeisser MJ, Ey E, Wegener S, Bockmann J, Stempel AV, Kuebler A, et al. Autistic-like behaviours and hyperactivity in mice lacking ProSAP1/Shank2. Nature. 2012; 486(7402):256–260. [PubMed: 22699619]

26. Giustetto M, Kirsch J, Fritschy JM, Cantino D, Sassoè-Pognetto M. Localization of the clustering protein gephyrin at GABAergic synapses in the main olfactory bulb of the rat. J Comp Neurol. 1998; 395(2):231–244. [PubMed: 9603375]
27. Calabresi P, Pisani A, Mercuri NB, Bernardi G. Long-term Potentiation in the Striatum is Unmasked by Removing the Voltage-dependent Magnesium Block of NMDA Receptor Channels. Eur J Neurosci. 1992; 4(10):929–935. [PubMed: 12106428]
28. Sala M, Braida D, Lentini D, Busnelli M, Bulgheroni E, Capurro V, et al. Pharmacologic rescue of impaired cognitive flexibility, social deficits, increased aggression, and seizure susceptibility in oxytocin receptor null mice: a neurobehavioral model of autism. Biol Psychiatry. 2011; 69(9):875–882. [PubMed: 21306704]
29. McFarlane HG, Kusek GK, Yang M, Phoenix JL, Bolivar VJ, Crawley JN. Autism-like behavioral phenotypes in BTBR T+tf/J mice. Genes Brain Behav. 2008; 7(2):152–163. [PubMed: 17559418]
30. Kenney JW, Adoff MD, Wilkinson DS, Gould TJ. The effects of acute, chronic, and withdrawal from chronic nicotine on novel and spatial object recognition in male C57BL/6J mice. Psychopharmacology (Berl). 2011; 217(3):353–365. [PubMed: 21487656]
31. Bevins RA, Besheer J. Object recognition in rats and mice: a one-trial non-matching-to-sample learning task to study 'recognition memory'. Nat Protoc. 2006; 1(3):1306–1311. [PubMed: 17406415]
32. Morris R. Developments of a water-maze procedure for studying spatial learning in the rat. J Neurosci Methods. 1984; 11(1):47–60. [PubMed: 6471907]
33. Zhang H, Zhang SB, Zhang QQ, Liu M, He XY, Zou Z, et al. Rescue of cAMP response element-binding protein signaling reversed spatial memory retention impairments induced by subanesthetic dose of propofol. CNS Neurosci Ther. 2013; 19(7):484–493. [PubMed: 23534694]
34. Verpelli C, Carlessi L, Bechi G, Fusar Poli E, Orellana D, Heise C, et al. Comparative neuronal differentiation of self-renewing neural progenitor cell lines obtained from human induced pluripotent stem cells. Front Cell Neurosci. 2013; 7:175. [PubMed: 24109433]
35. Kammermeier PJ, Xiao B, Tu JC, Worley PF, Ikeda SR. Homer proteins regulate coupling of group I metabotropic glutamate receptors to N-type calcium and M-type potassium channels. J Neurosci. 2000; 20(19):7238–7245. [PubMed: 11007880]
36. Kammermeier PJ, Worley PF. Homer 1a uncouples metabotropic glutamate receptor 5 from postsynaptic effectors. Proc Natl Acad Sci U S A. 2007; 104(14):6055–6060. [PubMed: 17389377]
37. D'Antoni S, Spatuzza M, Bonaccorso CM, Musumeci SA, Ciranna L, Nicoletti F, et al. Dysregulation of group-I metabotropic glutamate (mGlu) receptor mediated signalling in disorders associated with Intellectual Disability and Autism. Neurosci Biobehav Rev. 2014; 46(Pt 2):228–241. [PubMed: 24548786]
38. Hayashi MK, Tang C, Verpelli C, Narayanan R, Stearns MH, Xu RM, et al. The postsynaptic density proteins Homer and Shank form a polymeric network structure. Cell. 2009; 137(1):159–171. [PubMed: 19345194]
39. Verpelli C, Sala C. Molecular and synaptic defects in intellectual disability syndromes. Curr Opin Neurobiol. 2012; 22(3):530–536. [PubMed: 22000839]
40. Zitzer H, Honck HH, Bachner D, Richter D, Kreienkamp HJ. Somatostatin receptor interacting protein defines a novel family of multidomain proteins present in human and rodent brain. J Biol Chem. 1999; 274:32997–33001. [PubMed: 10551867]
41. Zitzer H, Richter D, Kreienkamp HJ. Agonist-dependent interaction of the rat somatostatin receptor subtype 2 with cortactin-binding protein 1. J Biol Chem. 1999; 274(26):18153–18156. [PubMed: 10373412]
42. Kinney GG, O'Brien JA, Lemaire W, Burno M, Bickel DJ, Clements MK, et al. A novel selective positive allosteric modulator of metabotropic glutamate receptor subtype 5 has in vivo activity and antipsychotic-like effects in rat behavioral models. J Pharmacol Exp Ther. 2005; 313(1):199–206. [PubMed: 15608073]
43. Pisani A, Gubellini P, Bonsi P, Conquet F, Picconi B, Centonze D, et al. Metabotropic glutamate receptor 5 mediates the potentiation of N-methyl-D-aspartate responses in medium spiny striatal neurons. Neuroscience. 2001; 106(3):579–587. [PubMed: 11591458]

44. Bonsi P, Platania P, Martella G, Madeo G, Vita D, Tassone A, et al. Distinct roles of group I mGlu receptors in striatal function. Neuropharmacology. 2008; 55(4):392–395. [PubMed: 18602651]
45. Lindsley CW, Wisnoski DD, Leister WH, O'brien JA, Lemaire W, Williams DL, et al. Discovery of positive allosteric modulators for the metabotropic glutamate receptor subtype 5 from a series of N-(1,3-diphenyl-1H- pyrazol-5-yl)benzamides that potentiate receptor function in vivo. J Med Chem. 2004; 47(24):5825–5828. [PubMed: 15537338]
46. Uslaner JM, Parmentier-Batteur S, Flick RB, Surles NO, Lam JS, McNaughton CH, et al. Dose-dependent effect of CDPPB, the mGluR5 positive allosteric modulator, on recognition memory is associated with GluR1 and CREB phosphorylation in the prefrontal cortex and hippocampus. Neuropharmacology. 2009; 57(5-6):531–538. [PubMed: 19627999]
47. Bozdagi O, Tavassoli T, Buxbaum JD. Insulin-like growth factor-1 rescues synaptic and motor deficits in a mouse model of autism and developmental delay. Mol Autism. 2013; 4(1):9. [PubMed: 23621888]
48. Drapeau E, Dorr NP, Elder GA, Buxbaum JD. Absence of strong strain effects in behavioral analyses of Shank3-deficient mice. Dis Model Mech. 2014; 7(6):667–681. [PubMed: 24652766]
49. Lee J, Chung C, Ha S, Lee D, Kim DY, Kim H, et al. Shank3-mutant mice lacking exon 9 show altered excitation/inhibition balance, enhanced rearing, and spatial memory deficit. Front Cell Neurosci. 2015; 9:94. [PubMed: 25852484]
50. Welch JM, Lu J, Rodriguiz RM, Trotta NC, Peca J, Ding JD, et al. Cortico-striatal synaptic defects and OCD-like behaviours in Sapap3-mutant mice. Nature. 2007; 448(7156):894–900. [PubMed: 17713528]
51. Langen M, Bos D, Noordermeer SD, Nederveen H, van Engeland H, Durston S. Changes in the development of striatum are involved in repetitive behavior in autism. Biol Psychiatry. 2014; 76(5):405–411. [PubMed: 24090791]
52. Duffney LJ, Zhong P, Wei J, Matas E, Cheng J, Qin L, et al. Autism-like Deficits in Shank3-Deficient Mice Are Rescued by Targeting Actin Regulators. Cell Rep. 2015; 11(9):1400–1413. [PubMed: 26027926]
53. Ronesi JA, Collins KA, Hays SA, Tsai NP, Guo W, Birnbaum SG, et al. Disrupted Homer scaffolds mediate abnormal mGluR5 function in a mouse model of fragile X syndrome. Nat Neurosci. 2012
54. Pignatelli M, Piccinin S, Molinaro G, Di Menna L, Riozzi B, Cannella M, et al. Changes in mGlu5 receptor-dependent synaptic plasticity and coupling to homer proteins in the hippocampus of Ube3A hemizygous mice modeling angelman syndrome. J Neurosci. 2014; 34(13):4558–4566. [PubMed: 24672001]
55. Kelleher RJ, Geigenmüller U, Hovhannisyan H, Trautman E, Pinard R, Rathmell B, et al. High-throughput sequencing of mGluR signaling pathway genes reveals enrichment of rare variants in autism. PLoS One. 2012; 7(4):e35003. [PubMed: 22558107]
56. Won H, Lee HR, Gee HY, Mah W, Kim JI, Lee J, et al. Autistic-like social behaviour in Shank2-mutant mice improved by restoring NMDA receptor function. Nature. 2012; 486(7402):261–265. [PubMed: 22699620]
57. Auerbach BD, Osterweil EK, Bear MF. Mutations causing syndromic autism define an axis of synaptic pathophysiology. Nature. 2011; 480(7375):63–68. [PubMed: 22113615]
58. Lin CW, Chen CY, Cheng SJ, Hu HT, Hsueh YP. Sarm1 deficiency impairs synaptic function and leads to behavioral deficits, which can be ameliorated by an mGluR allosteric modulator. Front Cell Neurosci. 2014; 8:87. [PubMed: 24744698]
59. Conn PJ, Lindsley CW, Meiler J, Niswender CM. Opportunities and challenges in the discovery of allosteric modulators of GPCRs for treating CNS disorders. Nat Rev Drug Discov. 2014; 13(9): 692–708. [PubMed: 25176435]

Europe PMC Funders Author Manuscripts

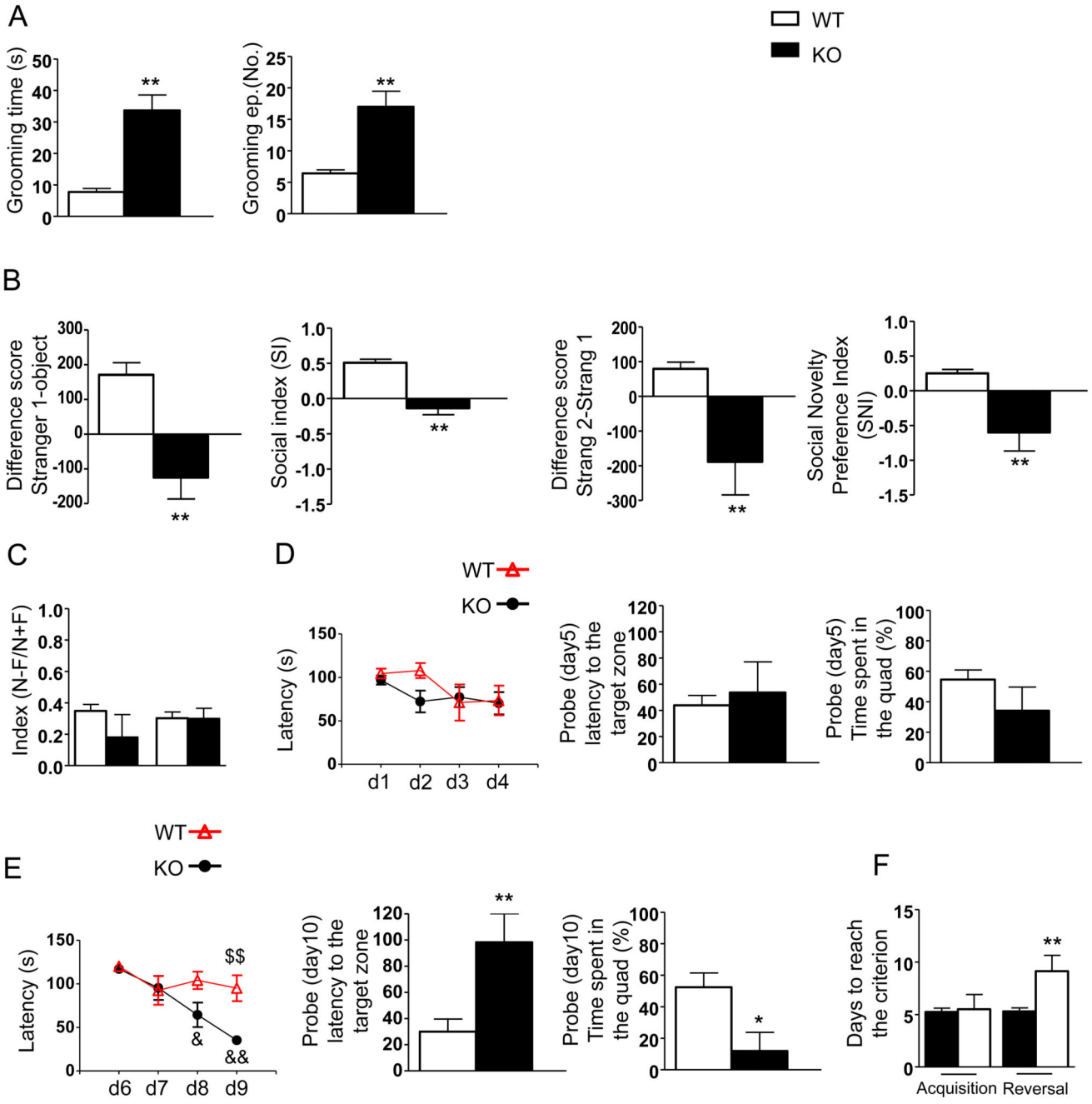

Figure 1.

Deletion of Shank3 in mice results in ASD-like behaviors. **A)** Self-grooming behavior was evaluated as the time spent grooming (left) and the total number of grooming episodes (right). **B)** Differences in scores obtained for time spent in the chamber associated with the never seen before mouse and the empty cage (left) or the familiar mouse (preference for social novelty test) (right). **C)** Spatial memory was evaluated by determining a discrimination index in the spatial object recognition test. **D-E)** Acquisition and reversal in the Morris water maze was analyzed to determine learning patterns (left), escape latency to

the target zone (center) and the time spent in the quadrant (right). **F)** Performance in the T maze test was analyzed as the number of days required to reach the criterion during the acquisition and reversal phases.

Data are shown as the mean ± SEM of 10 animals for each group. *, $p<0.05$, **, $p<0.01$; compared to the corresponding WT mice; $^{\$\$}$, $p<0.01$ compared to the corresponding WT mice on the same day; &&, $p<0.01$ compared to the same genotype on day 1. Student's t-tests or two-way Anova followed by Bonferroni tests were used for statistical analysis.

Europe PMC Funders Author Manuscripts

Europe PMC Funders Author Manuscripts

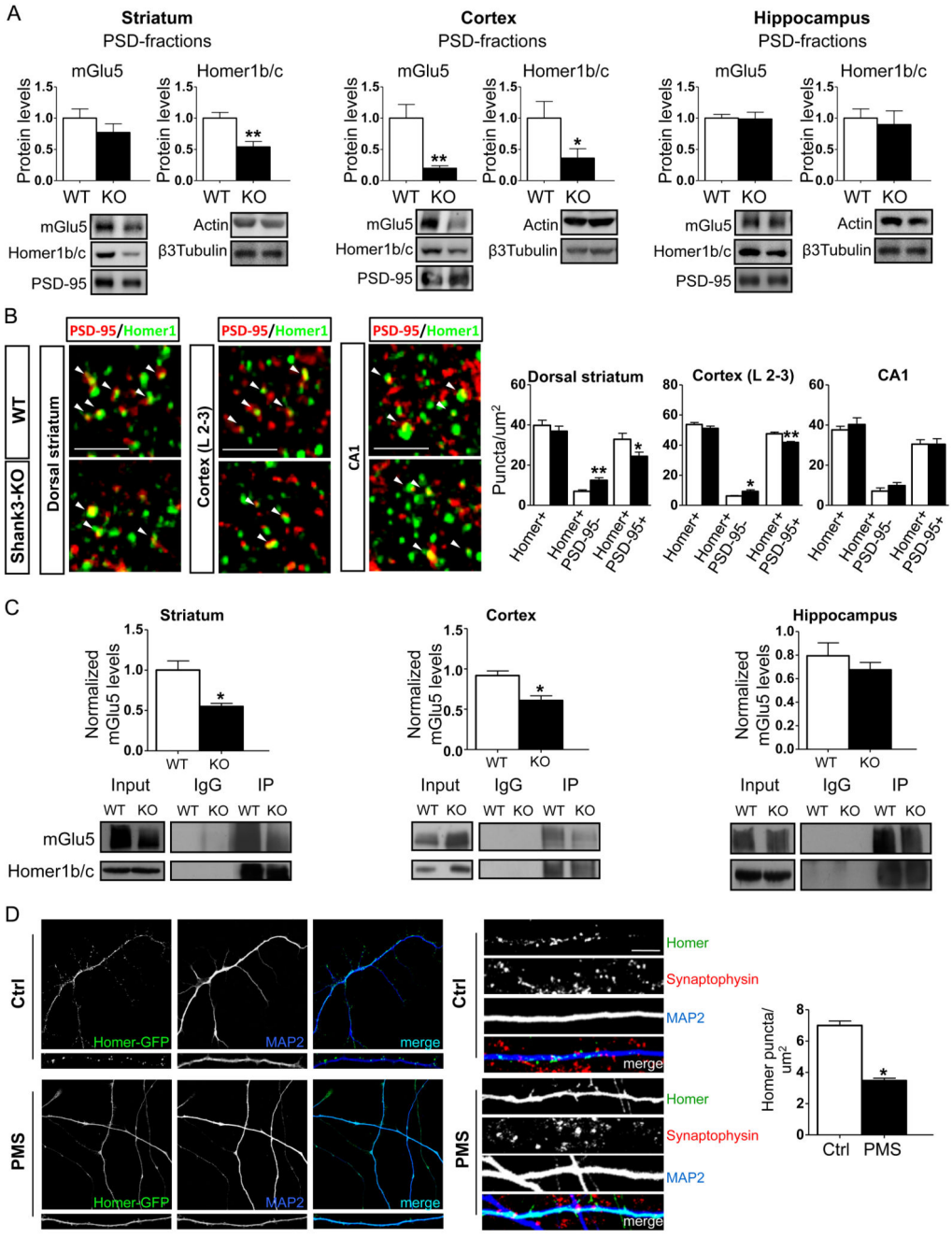

Figure 2.

Shank3 absence alters Homer and mGlu5 receptor synaptic localization. **A)** Protein levels of metabotropic glutamate receptor 5 (mGlu5) and Homer1b/c were analyzed using Western Blot analysis in postsynaptic density (PSD) fractions obtained from tissues in the striatum cortex and hippocampus of wild-type (WT) and *Shank3Δ11*$^{-/-}$ mice. Protein levels were each normalized against the respective PSD-95 and ratios were compared between genotypes. The results are shown as bar diagrams, and representative blots are shown below. All data are presented as the mean ± SEM; all P-values were derived using unpaired, two-tailed

Europe PMC Funders Author Manuscripts

Student's t-tests; *, p<0.05; **, p<0.01. Analyses are based on a sample size of n=6 animals for each group (WT and KO). **B)** Representative confocal micrographs showing PSD-95 (red) and Homer1 (green). Co-labeled puncta (arrowheads) are visible in high magnification images. The images show immunofluorescence puncta in the neuropil of the dorsal striatum, layer 2-3 of the primary somatosensory cortex and in the CA1 of the hippocampus in *Shank3Δ11*$^{-/-}$ and KO mice. The results are shown as bar diagrams. Data are presented as mean ± SEM. * p<0.05; ** p<0.01. Analyses are based on a sample size of n=6 animals for each group (WT and KO). Scale bars: 3 μm. **C)** PSD-enriched preparations of the striatum cortex and hippocampus were obtained from three P60 WT and KO mice and subjected to an in vitro immunoprecipitation assay using rabbit Homer1b/c antibodies. The immunoprecipitated proteins were revealed after immunoblotting using rabbit mGlu5 and Homer1 antibodies. A rabbit IgG antibody was used as the negative control. The data are expressed as the mean ± SEM of three independent experiments and we used n=2 animals for each group (WT and KO) and experiment. *, p<0.05. **D)** The panels show representative images of hNP-derived neurons and dendrites from control and PMS patients, which, after infection with a lentivirus expressing Homer-GFP, were differentiated in neuronal differentiation medium for 80 days. The staining (right panel) shows that GFP-Homer1b clusters in iPSC-derived neurons colocalize with the presynaptic marker Synaptophysin. Scale bar 10μm The results are shown as bar diagrams. The data are presented as the mean ± SEM of three independent experiments and we used n=2 independent hNP for each individuals. *, p<0.05.

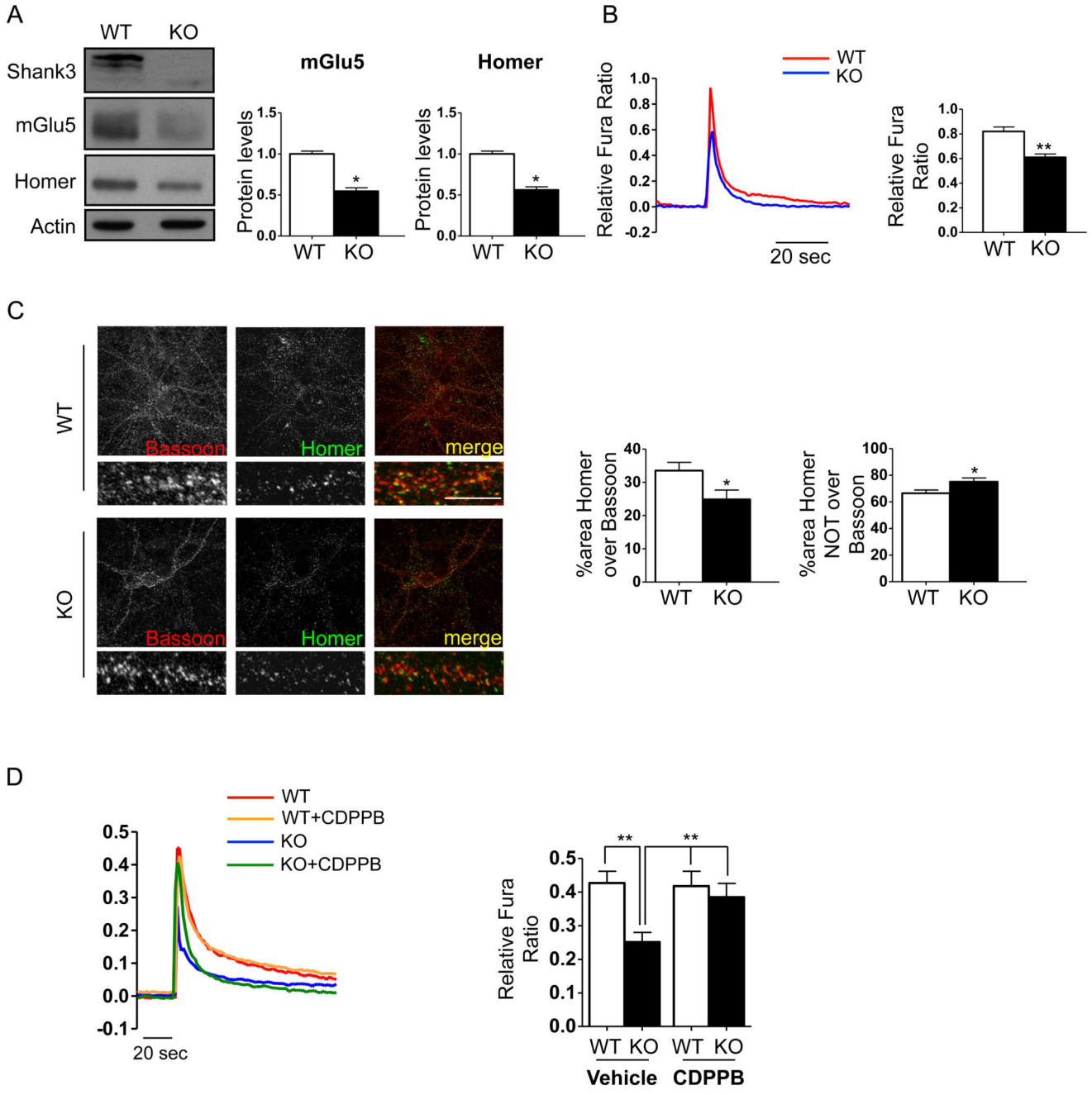

Figure 3.

Shank3 absence impairs mGlu5-mediated intracellular calcium release in cortical neurons. Cortical neuronal cultures were prepared from WT and *Shank3Δ11*$^{-/-}$ E17-E18 mouse embryos. **A)** Western blot analysis of PSD-enriched fractions of cortical primary neurons obtained from WT and *Shank3Δ11*$^{-/-}$ mice at DIV15. Protein levels were each normalized against the respective actin control. Data are expressed as the mean ± SEM of n=3 independent cultures by genotype. *, $p < 0.05$. **B)** At DIV14-15 neurons were loaded with Fura-2 AM (5 μM, 30 min). After 20 min of de-esterification, the neurons were challenged

Europe PMC Funders Author Manuscripts

with 200 μM DHPG. The results are shown as bar diagrams. Representative traces of Ca^{2+} transients are shown at the left, and the data are expressed as the mean ± SEM of n=127 WT neurons and n=151 KO neurons that were registered from 18 coverslips (for each genotype) in three independent cultures. *, p<0.05; **, p<0.01. **C)** Representative images of WT and *Shank3Δ11*$^{-/-}$ mouse primary cortical neurons at DIV15. Confocal images were obtained using a Confocal Microscope with a 63x objective and with sequential-acquisition set at a resolution of 1024 x 1024 pixels. A total of 16 WT and *Shank3Δ11*$^{-/-}$ primary cortical neurons at DIV15 were randomly chosen for quantification from 4 to 10 coverslips from three independent experiments. Colocalization measurements were performed using MetaMorph image analysis software. Scale bar 5μm . The histogram shows the mean ± SEM for the area of Homer clusters over the area of Bassoon clusters and the area of Homer clusters NOT over Bassoon clusters. *, p < 0.05. **D)** At DIV12-14 cortical neurons were loaded with Fura-2 and challenged with 200 μM DHPG either in presence (5 min preincubation) or in absence of of 3 μM CDPPB. Results are shown as bar diagrams. Representative traces of Ca^{2+} transients are shown left; data are expressed as mean ± SEM of n=86 WT neurons and n=77 KO neurons with vehicle and of n=96 WT neurons and n=95 KO neurons with CDPPB registered from 18 coverslips (for each conditions) in three independent cultures for genotype. * p < 0.05; ** p < 0.01.

Europe PMC Funders Author Manuscripts

Europe PMC Funders Author Manuscripts

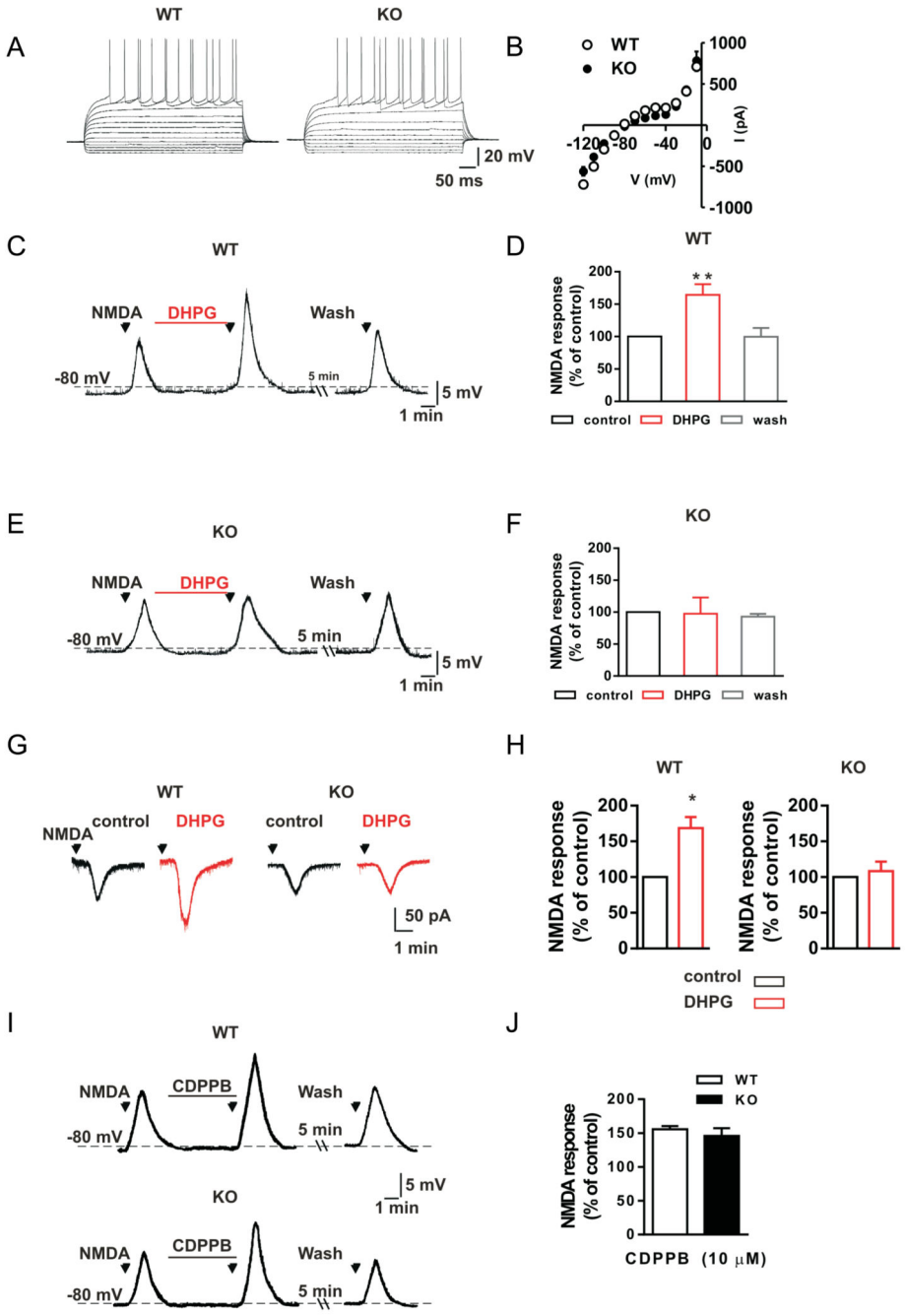

Figure 4.

The mGluR5-mediated enhancement of NMDA-induced neuronal responses is impaired in striatal medium spiny neurons of *Shank3Δ11*$^{-/-}$ mice **A)** Representative voltage traces show neuronal responses to hyperpolarizing and depolarizing current steps that were delivered to a striatal medium spiny neuron (MSN) in either a wild-type (WT) or a *Shank3Δ11*$^{-/-}$ (KO) mouse. **B)** The current-voltage plot for the MSNs that were recorded from WT and KO mice show that there was no difference between the two groups of mice ($p>0.05$), analyses are based on a sample size of n=5 animals for each group (WT and KO). **C, E)** Voltage traces

for MSNs that were recorded from WT (C) and a KO (E) mice show that the voltage responses when a 30 μM NMDA bath was applied to a striatal slice for 30 seconds under control conditions or in the presence of 50 μM of the mGluRI agonist DHPG for 5 minutes and after DHPG washout. **D, F)** Histograms show the NMDA-induced membrane depolarizations of MSNs recorded from WT (D) and KO (F) mice that were produced under control conditions, after 5 minutes of DHPG application, and following DHPG washout. ** $p<0.01$, analyses are based on a sample size of n=5 animals for each group (WT and KO). **G)** Current traces for two MSNs that were recorded from a WT (left) and a KO mouse (right) show the inward current that was produced when 30 μM NMDA was applied for 30 seconds under control conditions or in the presence of 50 μM DHPG. **H)** A histogram showing the NMDA-mediated inward current of MSNs from WT (left) and KO mice (right) in the presence of DHPG as a percentage of the response measured in the presence of NMDA alone. * $p<0.05$, analyses are based on a sample size of n=5 animals for each group (WT and KO). **I)** Voltage traces of two MSNs recorded from a WT (top) and a KO mouse (bottom) showing the voltage response produced by NMDA application in control condition and in the presence of 10 μM of the mGluR5 selective allosteric agonist CDPPB. **J)** Histogram showing the NMDA-mediated voltage response of MSNs from WT and KO mice in the presence of CDPPB as a percentage of the response measured in the presence of NMDA alone. Plot shows that there was no difference between the two groups of mice ($p>0.05$), analyses are based on a sample size of n=5 animals for each group (WT and KO)

Europe PMC Funders Author Manuscripts

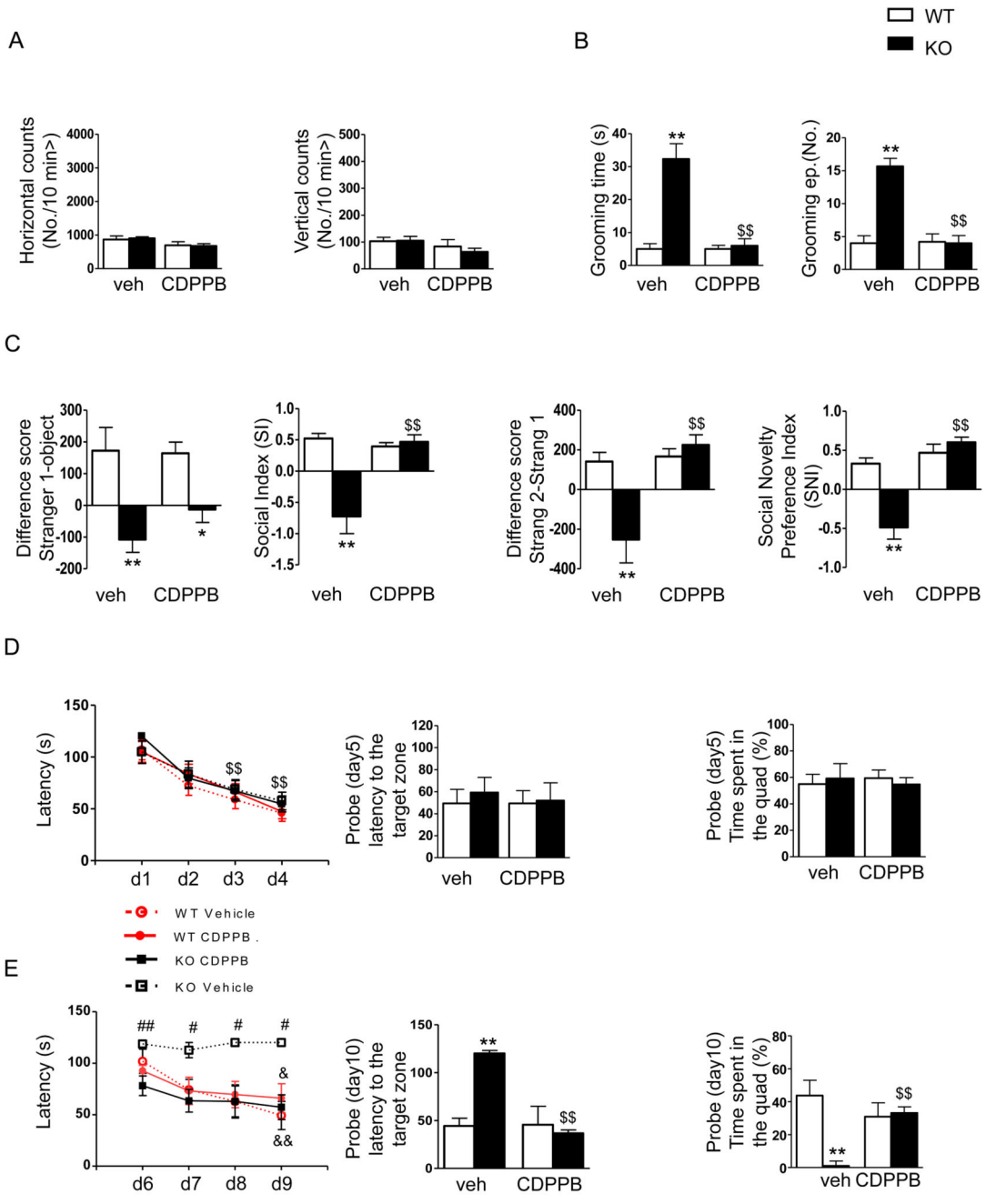

Figure 5.

The mGlu5 receptor positive agonist CDPPB rescues ASD-like behavior in *Shank3Δ11*$^{-/-}$ mice. The behavioral profiles of *Shank3Δ11*$^{-/-}$ mice were evaluated after treatment with CDPPB (3 mg/kg i.p.) or vehicle (veh), which were administered acutely or chronically at 70 min before each test. **A)** Mean horizontal (left) and vertical (right) movements were recorded for 10 min in an automated activity cage immediately after grooming recording. **B)** Self-grooming behaviors were evaluated as the time spent grooming (left) and the total number of grooming episodes (right) after acute treatment with CDPPB or vehicle. **C)**

Differences in the scores corresponding to the time spent in the chamber associated with the never-seen-before mouse and the empty cage (left) or the familiar mouse (preference for social novelty test) (right). **D-E)** Acquisition and reversal tasks in the Morris water maze were performed after daily treatments for the duration of the task during both acquisition and reversal in mice administered CDPPB or vehicle to analyze learning patterns (left), escape latency to the target zone (center) and the time spent in the quadrant (right) during the probe test. The data are shown as the mean ± SEM of n=13 animals for each group. *, $p < 0.05$; **, $p<0.01$ compared to the corresponding WT mice; $^{\$\$}$, $p<0.01$ compared to the corresponding *Shank3Δ11*$^{-/-}$ mice that were treated with vehicle; #, $p<0.05$ and ##, $p<0.01$ compared to the *Shank3Δ11*$^{-/-}$ mice that were treated with CDPPB. &, $p<0.05$ and &&, $p<0.01$ compared to the same genotype on day 1 (two-way Anova followed by Bonferroni test).

Europe PMC Funders Author Manuscripts